A new fixture for fracture tests under mixed mode I/II/III loading

S.M.J. Razavi*, F. Berto

Department of Mechanical and Industrial Engineering, Norwegian University of Science and Technology (NTNU), Richard Birkelands vei 2b, 7491 Trondheim, Norway

Abstract

In this paper, a new loading device for general mixed mode I/II/III fracture tests is designed and recommended. Finite element analyses are conducted on the proposed apparatus to evaluate the fracture parameters of the tested samples under various mixed mode loading conditions. The numerical results revealed that the designed loading fixture can generate wide varieties of mode mixities from pure tensile mode to pure in-plane and out of plane shear modes. The accuracy of the proposed fixture is evaluated by conducting a wide range of fracture tests on Compact Tension Shear (CTS) specimens made of polymethyl methacrylate (PMMA). The experimental results are then compared to the theoretical predictions obtained by the Richard criterion. A good consistency is observed between the experimental results and theoretical predictions.

Keywords: Brittle fracture; Fracture toughness; Mixed mode I/II; Mixed mode I/III; Mixed mode II/III; Mixed mode I/II/III.

Nomenclature	
a	crack length
E	elastic modulus
F	applied load
F_c	fracture load
K_I	mode I stress intensity factor
K_{II}	mode II stress intensity factor
K_{III}	mode III stress intensity factor

* Corresponding author. E-mail: javad.razavi@ntnu.no

K_{IC}	mode I fracture toughness
K_{IIC}	mode II fracture toughness
K_{IIIC}	mode III fracture toughness
K_{If}	critical mode I stress intensity factor
K_{IIf}	critical mode II stress intensity factor
K_{IIIf}	critical mode III stress intensity factor
K_{eff}	effective stress intensity factor
$K_{eff}\|_f$	effective stress intensity factor under fracture load
K_v	fracture limit surface
$O(r^{1/2})$	higher-order terms of stress field
(r, θ, z)	cylindrical coordinates
t	thickness of test specimen
U_i, UR_i (i: X, Y, Z)	symbols indicating translational and rotational degrees of freedom
W	width of test specimen
(X, Y, Z)	Cartesian coordinates
Y_I	mode I geometry factor
Y_{II}	mode II geometry factor
Y_{III}	mode III geometry factor
α	loading angle in C-fixture
β	loading angle in J-fixture
θ_f	in-plane crack kinking angle
v	Poisson's ratio
σ_{ij} (i, j: r, θ, z)	stress components
ϕ_f	out of plane crack kinking angle
CNC	computer numerical control
CTS	compact tension shear
FE	finite element
PMMA	Polymethyl methacrylate
SIF	stress intensity factor

1. Introduction

Brittle and ductile fracture are among the main categories of failure modes in real life components, hence a large number of researches have been conducted in this field. Due to its importance, the majority of the conducted researches are dedicated to the pure tensile mode of fracture, namely mode I fracture. However, numerous test specimens and testing procedures have been suggested to obtain the fracture behavior of different materials under a combination of tensile mode and in-plane shear mode (i.e. mixed mode I/II).[1-15] Applying different loading angles to the common pre-cracked specimens or considering angled pre-cracks in the test samples under mode I loading were suggested as solutions to get mixed mode I/II fracture properties. Among various test specimens for mixed mode I/II fracture experiments, one can suggest the angled edge crack specimen,[1] the compact tension-shear (CTS) specimen,[2-4] the rectangular plate containing an inclined center crack and subjected to a uniform far field tension,[5,6] the Brazilian disk specimen with central crack,[7,8] the asymmetric three/four-point bend specimen,[9-13] and the cracked semi-circular bend specimen,[14,15] which have been frequently used for mixed mode I/II fracture tests on different engineering materials such as ceramics and rocks, polymers and metals.

In addition to the researches on classic case of mixed mode I/II fracture, some experimental studies were conducted by researchers to consider the effect of tearing mode of fracture (i.e. mode III) on fracture behavior of pre-cracked components.[16-23] Compared to the case of mixed mode I/II, relatively fewer test procedures are available for mixed mode I/III loading. For examples, the plate with inclined crack through the thickness under a uniform far field tension,[16] the three-point bend specimen with an out of plane angled crack,[17] the compact tension (CT) specimen with inclined crack through the thickness,[18, 19] the traditional CT specimen subjected to combined tension-tear,[20] the circumferentially notched round bar,[21] the three-point bend specimen with asymmetrically oriented crack,[22] and the single edge cracked specimen under tensile/tear loading[23] are some of the specimens, which have been employed by researchers for mixed mode I/III fracture tests on different materials.

Beside the mentioned mixed mode conditions, there are some cases that the components are subjected to a mixture of in-plane and out of plane shear loading (i.e. mixed mode II/III), among which one can mention the cracks in railways, railway wheels and gears.[24, 25] Few researches are available in open literature dealing with the mixed mode II/III fracture test using testing rigs.[26-28]

Although the results of mixed mode I/II, I/III and II/III fracture tests give valuable knowledge about the overall behavior of material in presence of defects, however, considering the real-life components, a combination of all three modes of fracture (i.e. mode I, mode II and mode III) can results in final failure of the parts. As a matter of fact, performing mixed mode I/II/III fracture tests requires complex samples geometries and loading conditions. Hence, there are very limited test configurations for experimental investigation of mixed mode I/II/III fracture.[29-31] In order to have mixed mode fracture in pre-cracked components two different methods can be used; creating an angled pre-crack and applying the load (tensile or bending) or applying the load with a specific angle to a symmetrically pre-cracked specimen. In this research a testing fixture has been proposed, which allows to use traditional CTS specimens for complex mixed mode fracture tests. The proposed apparatus and the test sample have simple configuration, inexpensive fabrication procedure, convenience of testing set up and also the ability of introducing general mode mixities ranging from pure mode I to pure mode II and pure mode III. First the fracture testing fixture and test configuration is described and then its capabilities and accuracy are investigated by means of numerical simulations. Finally, a wide set of fracture tests are performed on Polymethyl methacrylate (PMMA) samples to practically check the fixture.

2. New loading fixture for mixed mode I/II/III fracture tests

Fig. 1 illustrates the geometry of new loading fixture and the test sample proposed for mixed mode I/II/III fracture experiments. The fixture includes two separate parts namely C-fixture and J-fixture (see Fig. 1). While C-fixture is used for applying in-plane shear load, J-fixture is used to apply out of plane shear load. Depending on the angle of rotation in each fixture different 3D mode mixities can be obtained. As shown in Fig. 1(b,c), five loading holes with equal angular position are drilled on each half of both C- and J-fixture. CTS geometry has been considered for the mixed mode tests (see Fig. 1c). The test specimen is fixed in the fixture using three pins on each side of sample. In order to eliminate possible plastic deformation around the loading holes and wear between different parts, the whole loading fixture was made of high strength abrasion resistant BRINAR® 450 steel considering a thickness of 20 mm for both inner and outer fixture. The positions of loading holes were chosen in a way to have a wide range of mode mixites among pure mode I ($\alpha = 0^{\circ}, \beta = 0^{\circ}$), pure mode II ($\alpha = 90^{\circ}, \beta = 0^{\circ}$) and pure mode III ($\alpha = 0^{\circ}, \beta = 90^{\circ}$) (see Fig. 2).

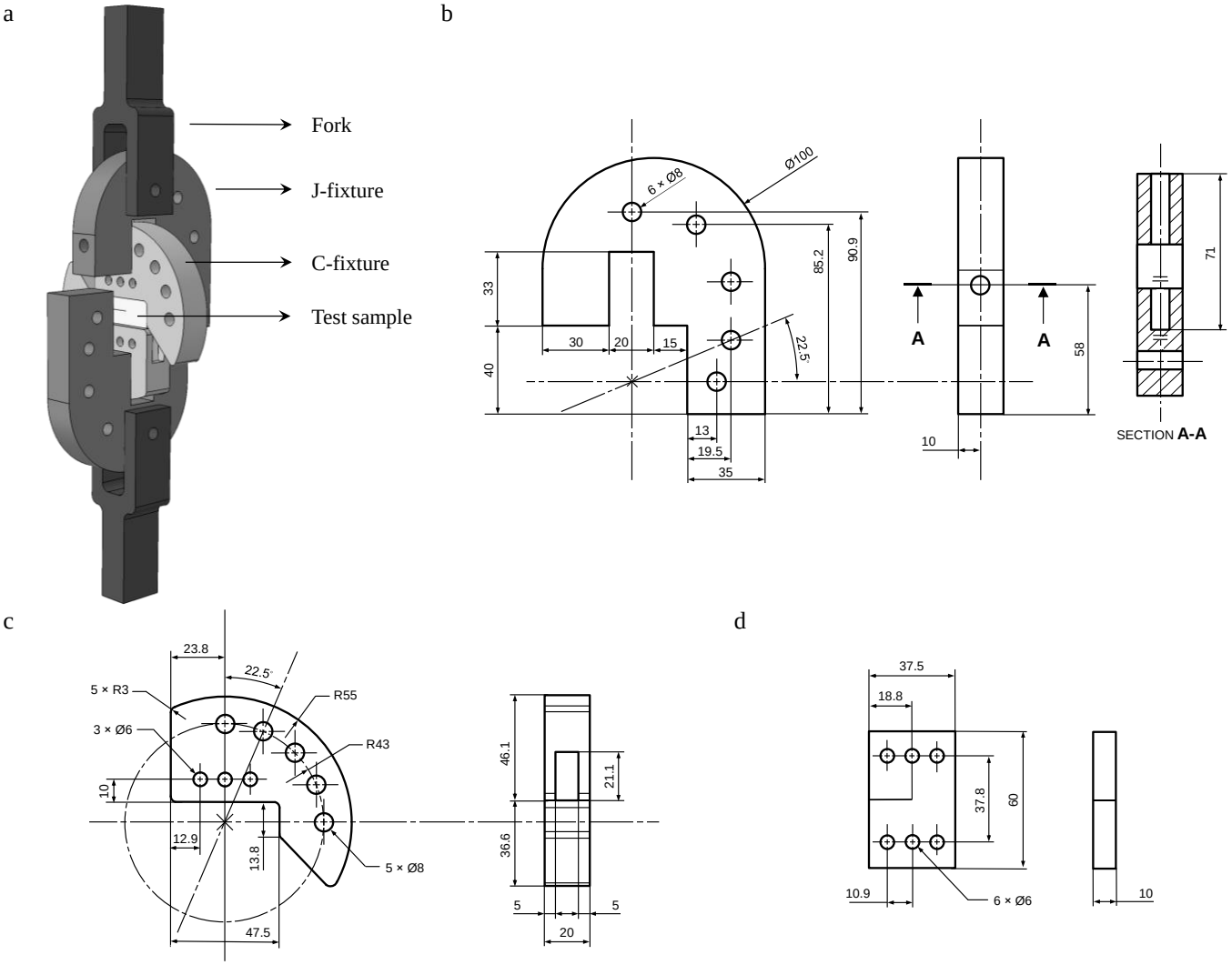

Fig. 1. (a) Schematic view of mixed mode I/II/III loading configuration, (b) J-fixture, (c) C-fixture, and (d) CTS specimen (dimensions in mm).

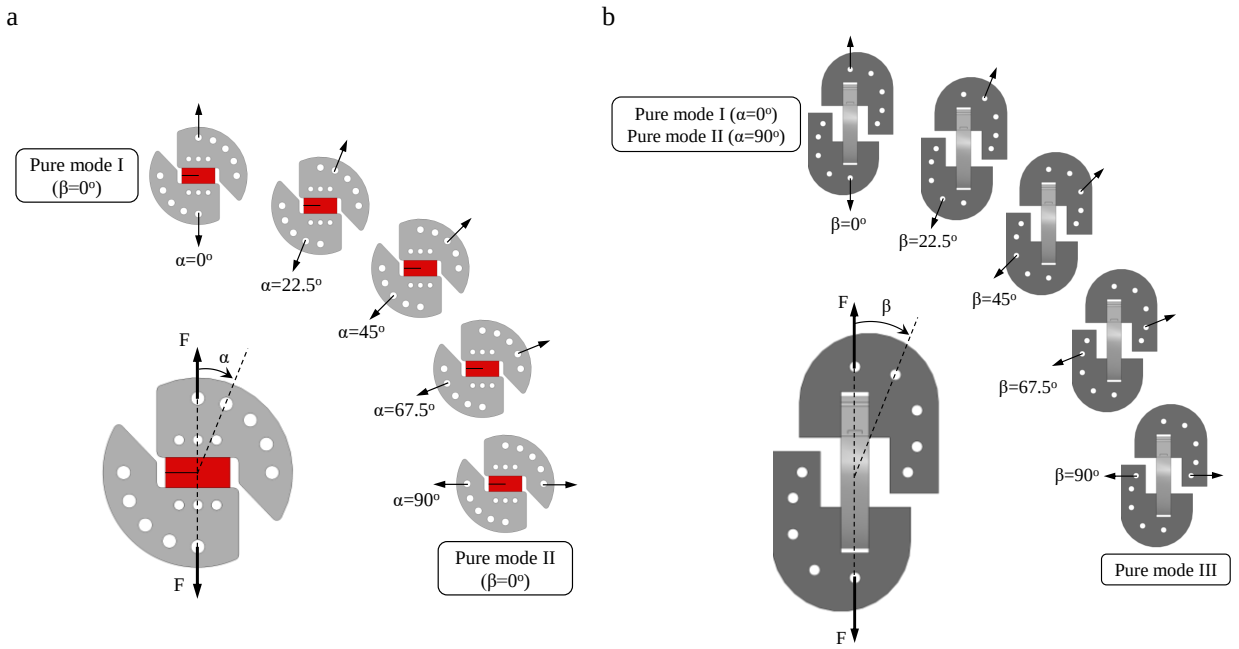

Fig. 2. Schematic view of (a) mixed mode I/II loading condition and (b) mixed mode I/III and mixed mode II/III loading conditions.

3. Theoretical background

The stress field around the crack tip in a component under complex loading can be described by near-field solutions using the superposition of all three modes of fracture. For a linear elastic homogeneous material, the crack tip stress field can be written as:

$$
\begin{aligned}
\sigma_{rr} &= \frac{1}{\sqrt{2\pi r}}\left[\frac{K_I}{4}\left(5\cos\frac{\theta}{2}-\cos\frac{3\theta}{2}\right)+\frac{K_{II}}{4}\left(-5\sin\frac{\theta}{2}+3\sin\frac{3\theta}{2}\right)\right]+O\left(r^{1/2}\right)\\
\sigma_{\theta\theta} &= \frac{1}{\sqrt{2\pi r}}\left[\frac{K_I}{4}\left(3\cos\frac{\theta}{2}+\cos\frac{3\theta}{2}\right)+\frac{K_{II}}{4}\left(-3\sin\frac{\theta}{2}-3\sin\frac{3\theta}{2}\right)\right]+O\left(r^{1/2}\right)\\
\sigma_{r\theta} &= \frac{1}{\sqrt{2\pi r}}\left[\frac{K_I}{4}\left(\sin\frac{\theta}{2}+\sin\frac{3\theta}{2}\right)+\frac{K_{II}}{4}\left(\cos\frac{\theta}{2}+3\cos\frac{3\theta}{2}\right)\right]+O\left(r^{1/2}\right)\\
\sigma_{\theta z} &= \frac{K_{III}}{\sqrt{2\pi r}}\cos\frac{\theta}{2}+O\left(r^{1/2}\right)\\
\sigma_{rz} &= \frac{K_{III}}{\sqrt{2\pi r}}\sin\frac{\theta}{2}+O\left(r^{1/2}\right)\\
\sigma_{zz} &= \begin{cases}0, & \text{Plane stress}\\ \nu\left(\sigma_{rr}+\sigma_{\theta\theta}\right), & \text{Plane strain}\end{cases}
\end{aligned}
\tag{1}
$$

in which, (r, θ, z) are the cylindrical coordinates shown in Fig. 3, K_I, K_{II}, and K_{III} are the mode I, mode II, and mode III stress intensity factors (SIF), and v is the Poisson's ratio. The higher-order terms of stress field, $O(r^{1/2})$, are often negligible near the crack tip for majority of the geometries. In order to simplify presentation of the fracture parameters, dimensionless form of SIF is introduced and used in the current research as given below

$$Y_i = \frac{K_i W t}{F\sqrt{\pi a}}, \qquad i = I, II, III \tag{2}$$

where Y_i is the geometry factor, W is the CTS width, t is the CTS thickness, F is the applied load, and a is the crack length.

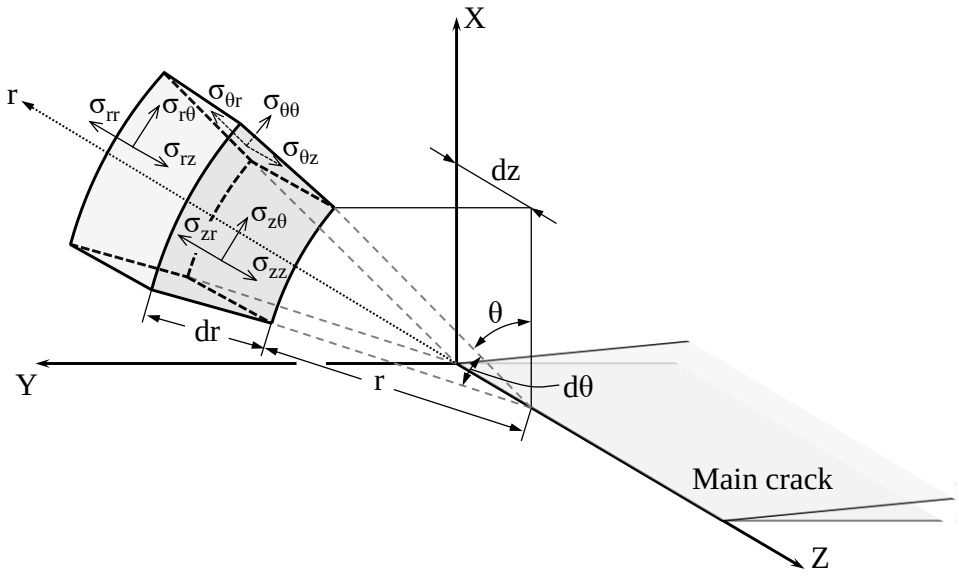

Fig. 3. Mixed mode I/II/III stress fields in the vicinity of the crack tip.

General mixed mode I/II/III problems are often characterized by the superposition of the pure mode I, mode II and mode III loading conditions. This means that the SIFs obtained under pure modes are used as the key parameter in fracture assessment of the complex crack geometries and/or complex loading conditions. Numerous fracture criteria have been proposed by researchers to predict the onset of brittle fracture under mixed mode I/II/III.[30, 32-38] In the current research, Richard criterion[30] was employed to evaluate the fracture data obtained using the proposed testing

set-up. According to this criterion, sudden fracture will occur if the local stress condition along the crack front reaches a point on the fracture limit surface, K_v. This can mathematically be expressed by the following expression:

$$K_v = \frac{K_I}{2} + \frac{1}{2}\sqrt{K_I^2 + 4\left(\alpha_1 K_{II}\right)^2 + 4\left(\alpha_2 K_{III}\right)^2} = K_{IC} \tag{3}$$

in which $\alpha_1=K_{IC}/K_{IIC}$ and $\alpha_2=K_{IC}/K_{IIIC}$, while K_{IC}, K_{IIC} *and* K_{IIIC} are the fracture toughness values under mode I, II and III.

Dealing with mixed mode I/II/III loading, fracture occurs in a plane which has an in-plane angle, θ_f and out of plane angle, ϕ_f with respect to the initial crack plane. Schematic view of fracture angles of a cracked component under different loading modes is displayed in Fig. 4. It is worth mentioning that the in-plane and out of plane fracture angles are caused by in-plane and out of plane shear loading, respectively. It is evident that for mixed mode I/II and I/III, the out of plane and in-plane fracture angles respectively is expected be equal to zero. These two fracture angles can be calculated using the following expressions for isotropic materials[30]:

$$\theta_f = \mp\left[A\frac{|K_{II}|}{K_I + |K_{II}| + |K_{III}|} + B\left(\frac{|K_{II}|}{K_I + |K_{II}| + |K_{III}|}\right)^2 \right] \tag{4}$$

where $\theta_f < 0^\circ$ for $K_{II} > 0$ and $\theta_f > 0^\circ$ for $K_{II} < 0$, and A=140° and B=-70°,

$$\phi_f = \mp\left[C\frac{|K_{III}|}{K_I + |K_{II}| + |K_{III}|} + D\left(\frac{|K_{III}|}{K_I + |K_{II}| + |K_{III}|}\right)^2 \right] \tag{5}$$

where $\phi_f < 0^\circ$ for $K_{III} > 0$ and $\phi_f > 0^\circ$ for $K_{III} < 0$, and C=78° and D=-33°.

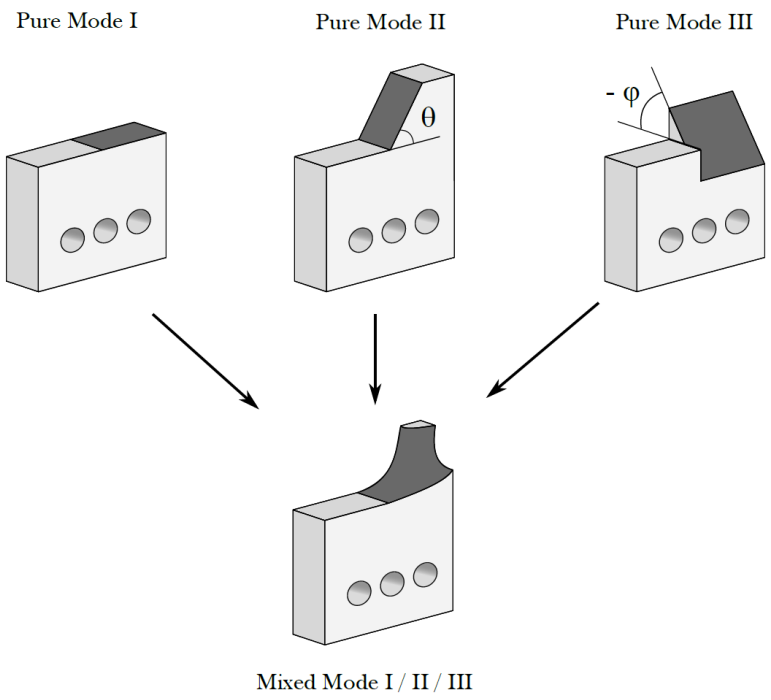

Fig. 4. In-plane and out of plane fracture angles.

4. Finite element analysis

4.1. Finite element model

Finite element models were developed in ABAQUS 6.14 standard finite element code to evaluate the new test fixture and to study the fracture parameters (K_I, K_{II} and K_{III}) under various mixed mode loading conditions. Although analytical methods might be available for stress intensity factors (SIF) calculation of simple test specimens, however, due to complex loading condition of the studied test specimens, finite element (FE) method was employed to obtain SIFs.

Three-dimensional linear elastic finite element analyses were conducted on the new test configuration. Due to considerable higher stiffness of the loading fixture compared to the PMMA specimens, they were modeled as rigid bodies. While, the PMMA specimens were modeled using their elastic material properties. The material properties of the tested PMMA obtained from tensile tests are presented in Table 1. Figs. 5a and 5b illustrate a typical finite element mesh pattern used for the FE model. The 10-node quadratic tetrahedron and 20-node quadratic brick elements were used for meshing the fixture parts and the test sample, respectively. The CTS specimen, C-fixture and J-fixture were attached to each other through bolt-holes. Singular elements of 80 μm size were used in the first ring of elements around the crack tip to produce the square root singularity of

stress/strain field. Eight elements were uniformly distributed along the CTS specimen to capture the variation of fracture parameters through the thickness. A mesh convergence study was performed by considering the SIF values as the key parameter to assure the sufficiency of the element size in the FE models. A total number of around 10,000 elements was used to mesh the CTS specimen.

Table 1. mechanical properties of PMMA.

Material property	
Elastic modulus, *E* (GPa)	2.9
Poisson's ratio, *v*	0.35
Ultimate strength (MPa)	66

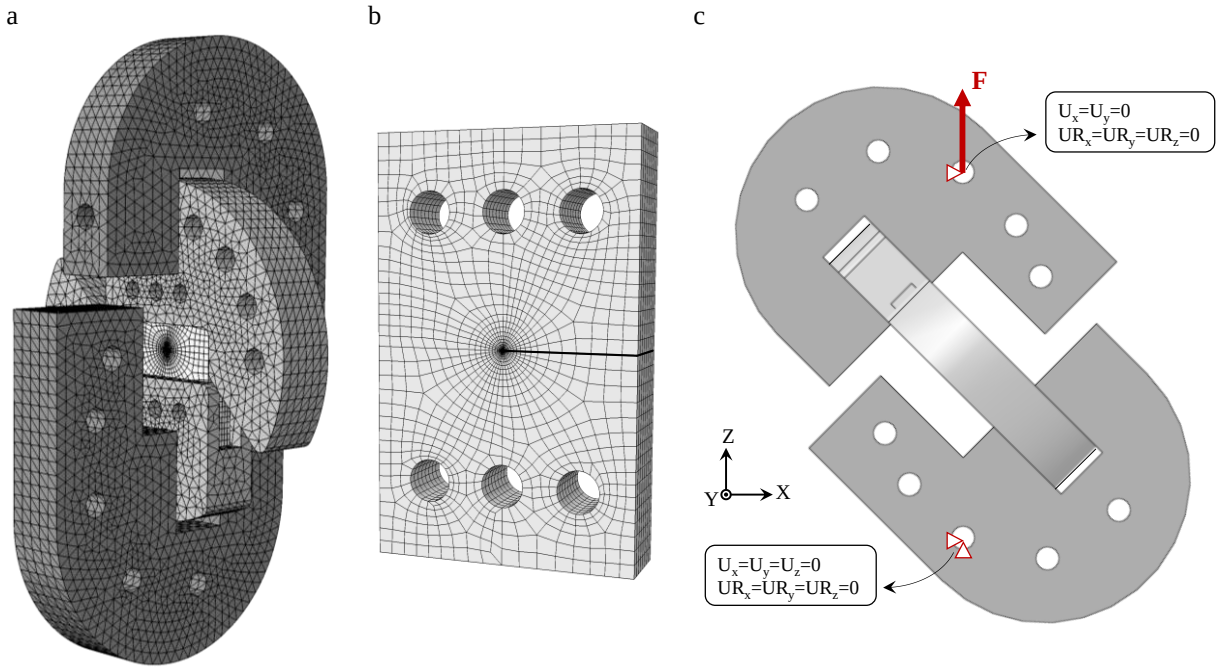

Fig. 5. (a) The finite element mesh pattern used for the numerical analysis of loading fixture and (b) CTS specimen (the bold line indicates the pre-crack) and (c) the boundary conditions applied to FE models (U_i and UR_i symbols indicate translational and rotational degrees of freedom, respectively).

Due to the contact between different parts, the frictionless "contact pairs" command (available in ABAQUS) was used in simulations, while beam elements were employed as pins, which are connecting the CTS specimen to C-fixture and C-fixture to J-fixture. Different mixed mode loading conditions were simulated by applying the load on different pairs of the loading holes. Fig. 5c shows the boundary conditions applied to the FE models. According to Fig. 5c, all the degrees

of freedom were constrained on the lower hole of J-fixture, while the upper hole was only free to move along the vertical direction. An interaction integral approach built in ABAQUS software was employed to obtain SIFs directly from the software.[39] The CTS specimen with an initial crack length of $a/W = 0.5$ was analyzed under 25 different loading modes.

4.2. Finite element results

The variation of the normalized SIFs along the crack front are illustrated in Figs. 6 and 7. For the sake of brevity, only some of the mixed mode conditions are presented. In these figures, t represents the specimen thickness and z indicates the position of each point along the crack front. According to Figs. 6, it can be observed that the variations of mode I geometry factor, Y_I along the crack front for the specimen under mode I loading (α=0°, β=0°) is symmetric and relatively uniform, however, its value decreases about 12% near the free surfaces of specimen, which results in a thumb-nail shaped crack front in specimens with high thickness. Unlike the previous case, the mode II geometry factor, Y_{II} along the crack front for the specimen under in-plane shear loading (α=90°, β=0°) has its peak values close to the free surface of specimen (also known as coroner points) (see Fig. 6). As a well-known fact in fracture mechanics, in-plane and out of plane shear modes of fracture (i.e. mode II and mode III, respectively) are coupled, which means that mode II or mode III loading of an elastic model with through-the thickness crack also generates a coupled three-dimensional mode III and mode II singular stress state, respectively[40-47] (see Fig. 8). As mentioned earlier by Pook[48], "*the nature of the crack tip singularity changes in the vicinity of a corner point, and these corner point singularities are an important source of three-dimensional effects*". It should be mentioned that for the specimens with higher thicknesses and materials with high Poisson's ratios, stronger corner point singularities and consequently stronger coupled fracture modes exist. Due to the couple modes of fracture, considerable mode III and mode II SIFs exist in the area close to the free surface of the specimens under mode II and mode III loadings (see Fig. 6), which results in higher effective SIFs (see Eq. 6) at both sides of the crack front in these cases. This increases the probability of crack initiation from both sides of crack front, which is consistent with the numerical and experimental findings reported by Zhu et al.[49] and Buchholz et al[50].

The effective stress intensity factor as a simplified measure of stress singularity under mixed mode loading can be defined as below:

$$K_{eff} = \sqrt{K_I^2 + K_{II}^2 + K_{III}^2} \tag{6}$$

Fig. 9 illustrates the normalized SIF variation with respect to the in-plane and out of plane loading angles. The normalized SIFs in Fig. 9 were obtained by dividing the SIFs to the effective SIFs at mid-section of the specimens. The elastic mode mixity parameters for different mixed mode conditions of I/II, I/III and II/III were defined according to Eq. 7-9. Based on the SIFs obtained at mid-section of the specimen, the mixed mode loading conditions provided by the presented loading fixture in the intermediate mixed mode I/II, I/III and II/III cases are M_{12}^e = 0.83, 0.63, 0.36, M_{13}^e = 0.92, 0.83, 0.66, and M_{23}^e =0.87, 0.72, 0.47, respectively.

$$M_{12}^e = \frac{2}{\pi}\tan^{-1}\left(\frac{K_I}{K_{II}}\right) \tag{7}$$

$$M_{13}^e = \frac{2}{\pi}\tan^{-1}\left(\frac{K_I}{K_{III}}\right) \tag{8}$$

$$M_{23}^e = \frac{2}{\pi}\tan^{-1}\left(\frac{K_{II}}{K_{III}}\right) \tag{9}$$

In order to better present each fracture mode portion in different loading condition, the normalized SIFs are separately presented in Fig. 10 for different loading angles (α and β). According to Fig. 10, pure mode I and pure mode II loading conditions can be obtained under (α=0°, β=0°) and (α=90°, β=0°) loading angles, while pure mode III can be obtained when β=90° independent of the C-fixture angle, α. Hence, in order to perform mode III fracture experiments using the new fixture, it would be enough to test the samples β=90° and only one angle of the C-fixture.

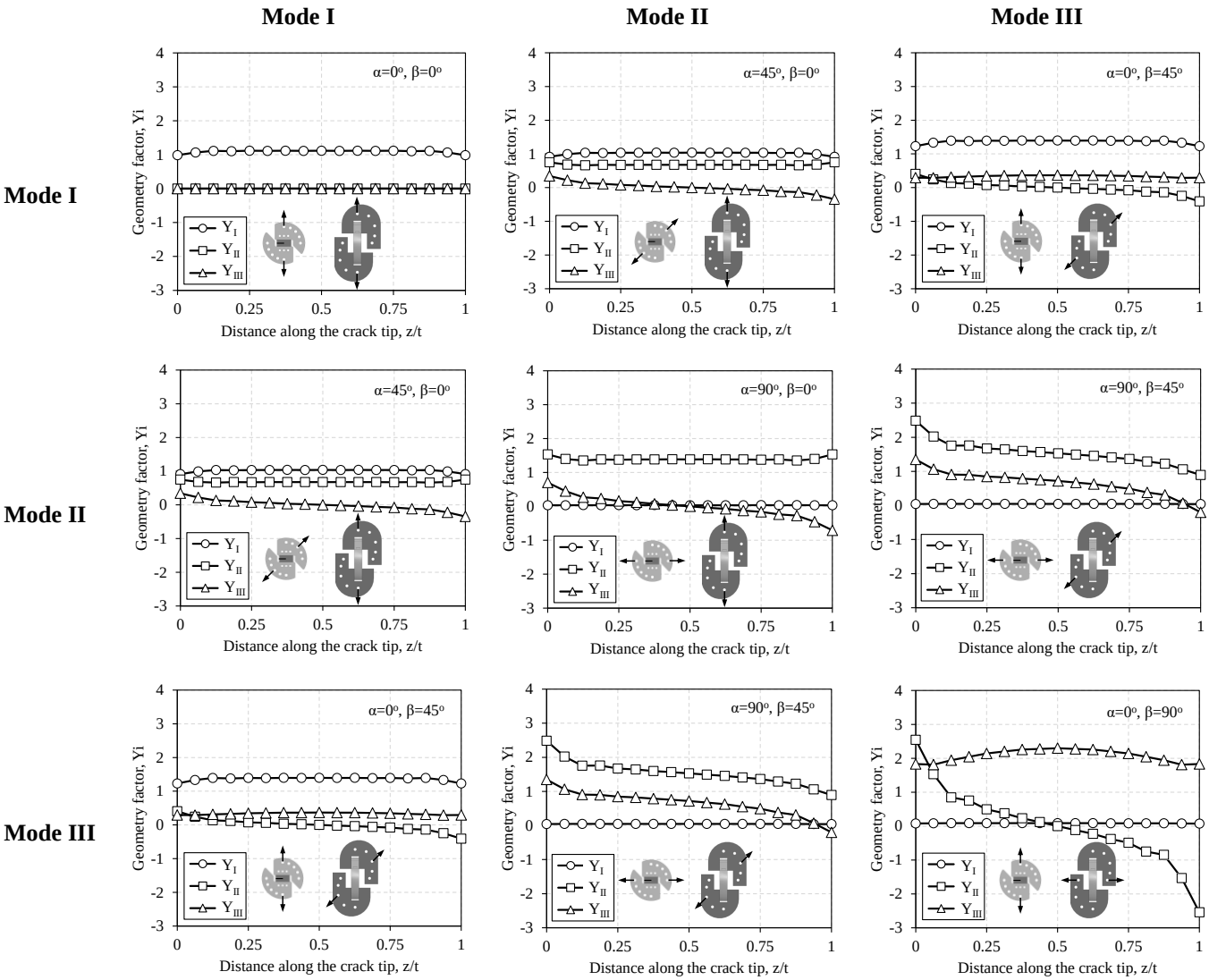

Fig. 6. The distribution of geometry factors along the crack front for different cases of planar mixed mode loading.

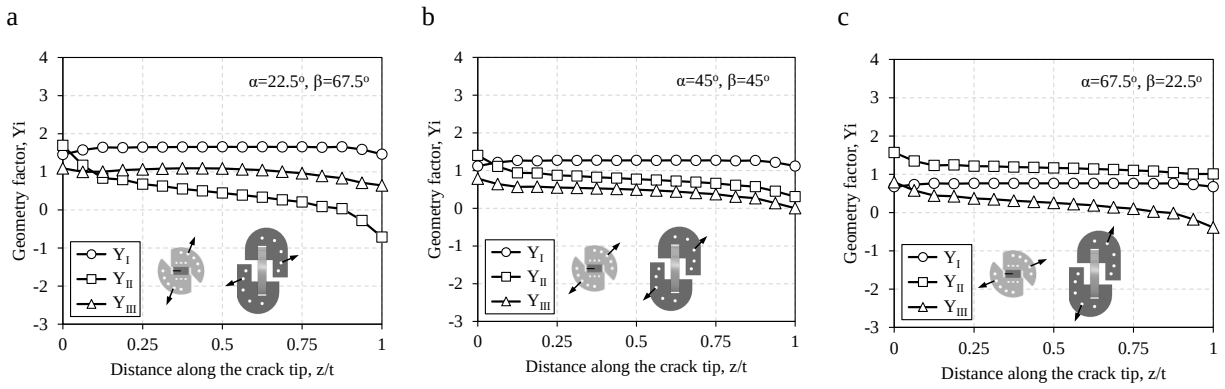

Fig. 7. The distribution of geometry factors along the crack front for different cases of mixed mode I/II/III.

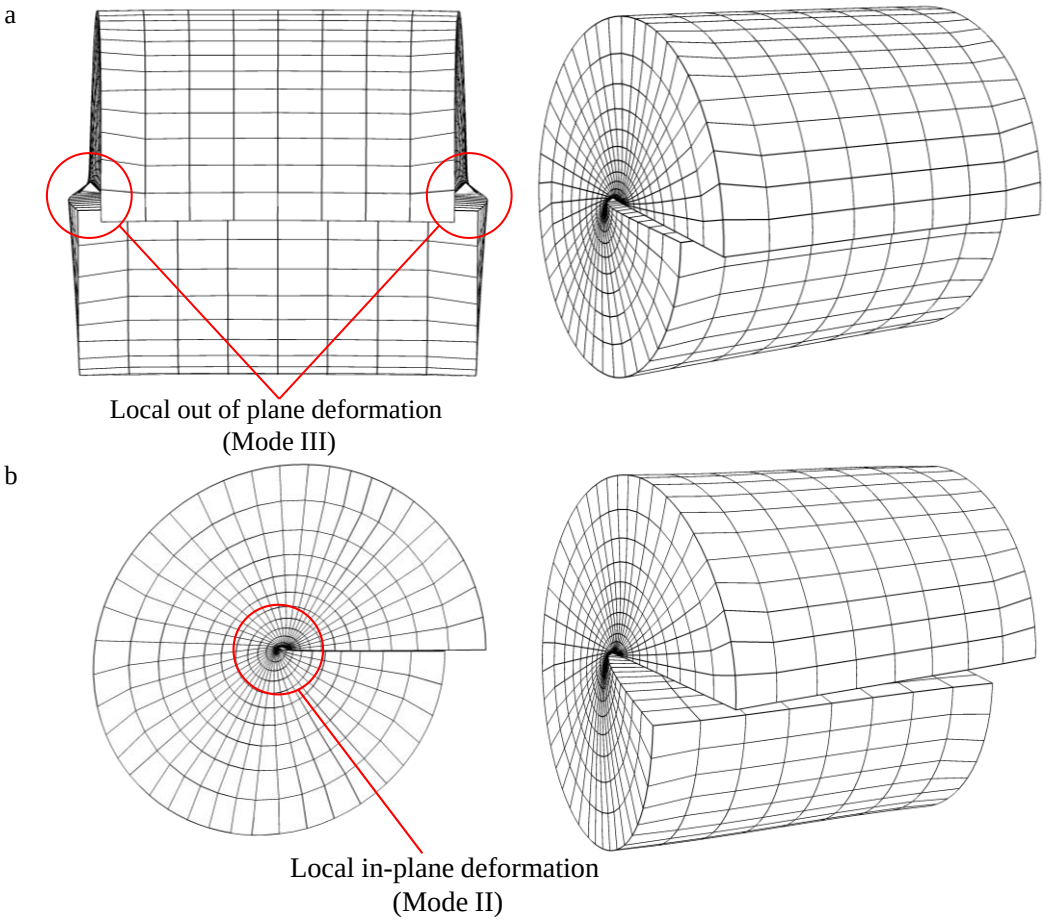

Fig. 8. An example of finite element results demonstrating the coupled modes of fracture; (a) induced out of plane deformation (i.e. mode III) in the model under in-plane shear loading (i.e. mode II), (b) induced in-plane deformation (i.e. mode II) in the model under out of plane shear loading (i.e. mode III).

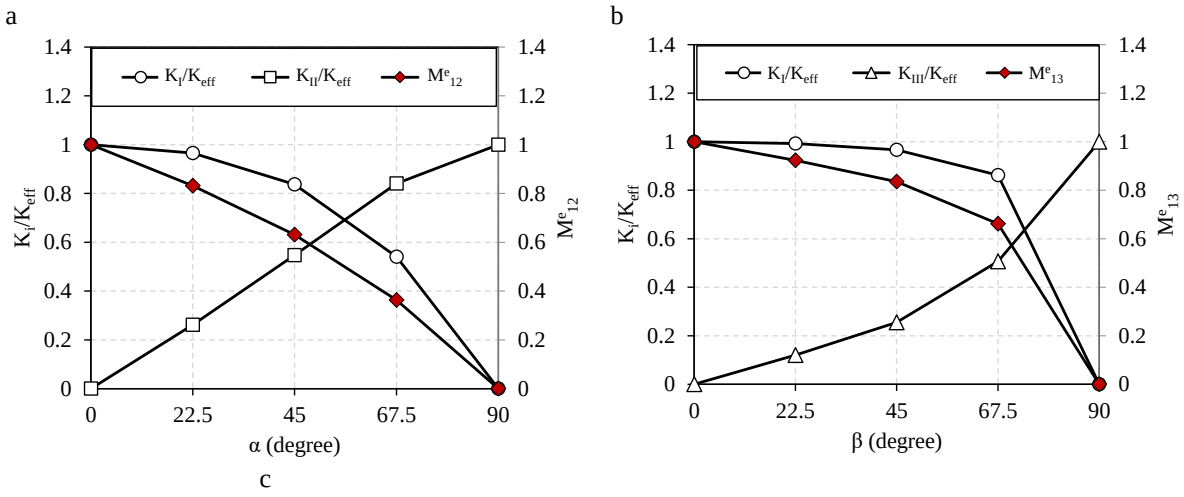

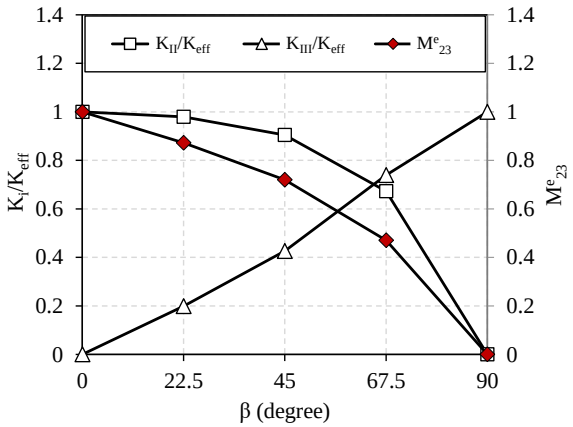

Fig. 9. The normalized SIFs and elastic mode mixity parameters for different loading conditions; (a) mixed mode I/II (β=0°), (b) mixed mode I/III (α=0°), and (c) mixed mode II/III (α=90°).

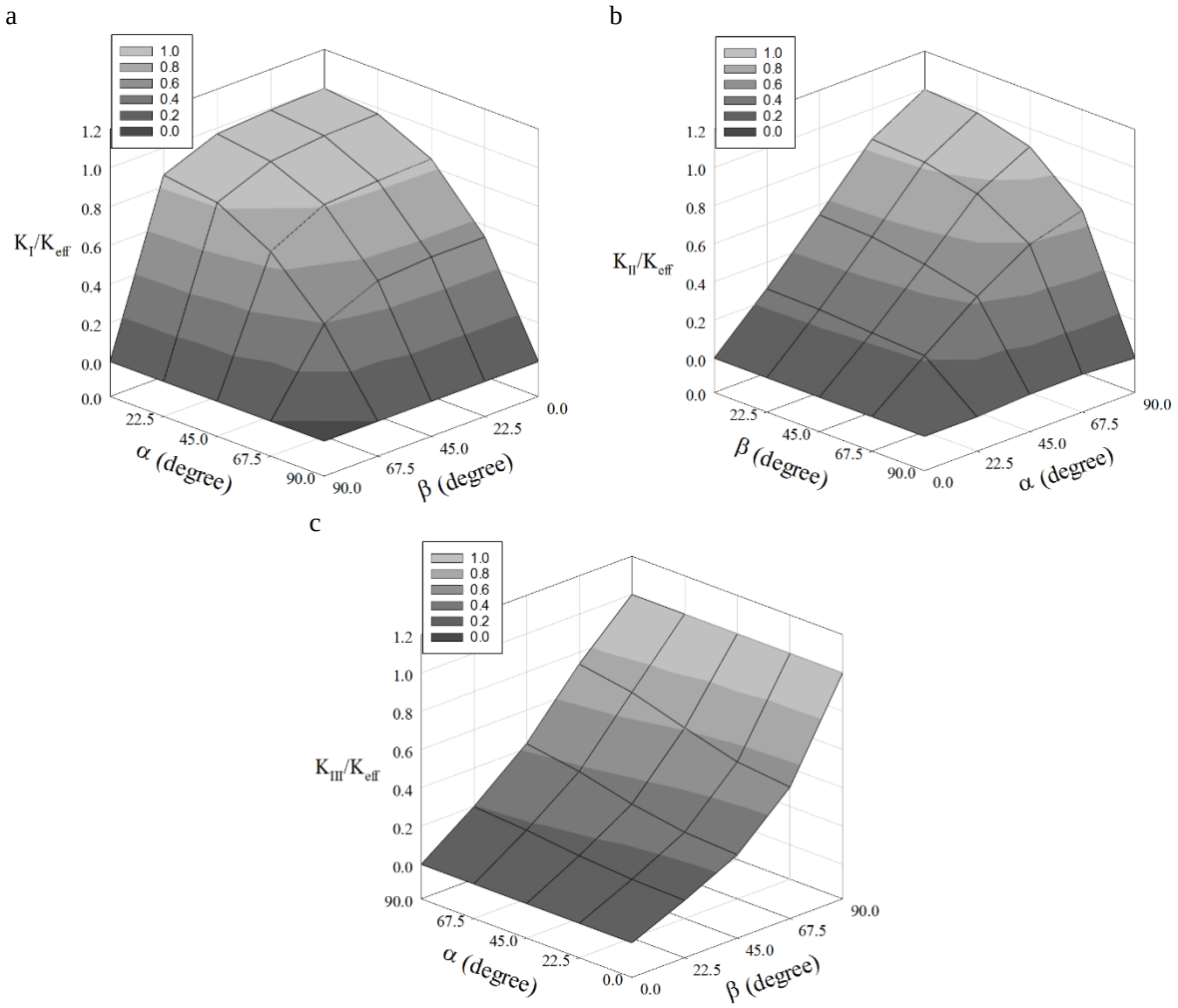

Fig. 10. The normalized SIFs under various loading conditions; (a) mode I SIF, (b) mode II SIF, and (c) mode III SIF.

5. Mixed mode fracture tests description

Polymethyl methacrylate (PMMA or Perspex) has been known by numerous researchers as a commonly used model material for performing fracture tests. PMMA is a transparent homogenous and isotropic material with linear elastic behavior at room temperature. Its brittle fracture behavior at room temperature, machinability and convenience of creating a sharp crack are among the advantages of PMMA in brittle fracture experiments.[51, 52]

According to the number of holes in C- and J-fixtures, 25 different loading conditions can be applied to the tests specimens. Hence, 80 CTS specimens were machined from a PMMA sheet of 10 mm thick and at least three tests were performed under each loading condition. Computer numerical control (CNC) machine was used for machining the border sides of the test specimens and 0.4 mm thick circular saw blade was used to create initial notch in the test specimens. For creating the sharp pre-crack, a razor blade was pressed carefully to make the final crack length of each specimen equal to $a/W = 0.5$. The depth of the pre-crack was carefully measured by an optical microscope (OptoSigma, osMS26-100, Tokyo-Japan) to ensure the precise crack length of the test specimens. Fig. 11 illustrates a typical PMMA specimen prepared for the fracture test. A series of fracture tests were performed on CTS specimens to examine the applicability and efficiency of the proposed loading fixture for mixed mode I/II/III fracture tests. Fracture tests were performed using 50 kN MTS machine (Minnesota-USA) under static loading at room temperature with a displacement rate of 1 mm/min. The external load was applied to the fixture using two forks connected to the J-fixture (see Fig. 12). This load was then transferred to the test specimen through three pins on each side of the specimen. The load displacement data were recorded during the tests. All the test samples were fractured suddenly from the crack tip and the load displacement curves represented linear behavior confirming the brittle fracture behavior of PMMA under various loading conditions. The representative load-displacement curves of CTS specimens under pure mode I, pure mode II, and pure mode III are displayed in Fig. 13. In-plane and out of plane fracture initiation angles were measured using high resolution optical microscope.

Fig. 11. A typical PMMA CTS test specimen.

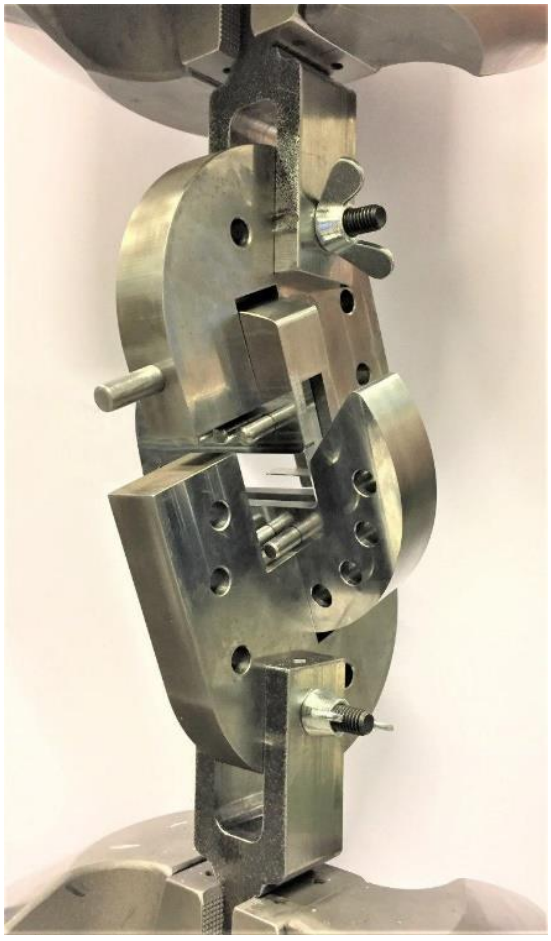

Fig. 12. loading set up used for mixed mode I/II/III fracture tests (α=0˚, β=22.5˚).

a b

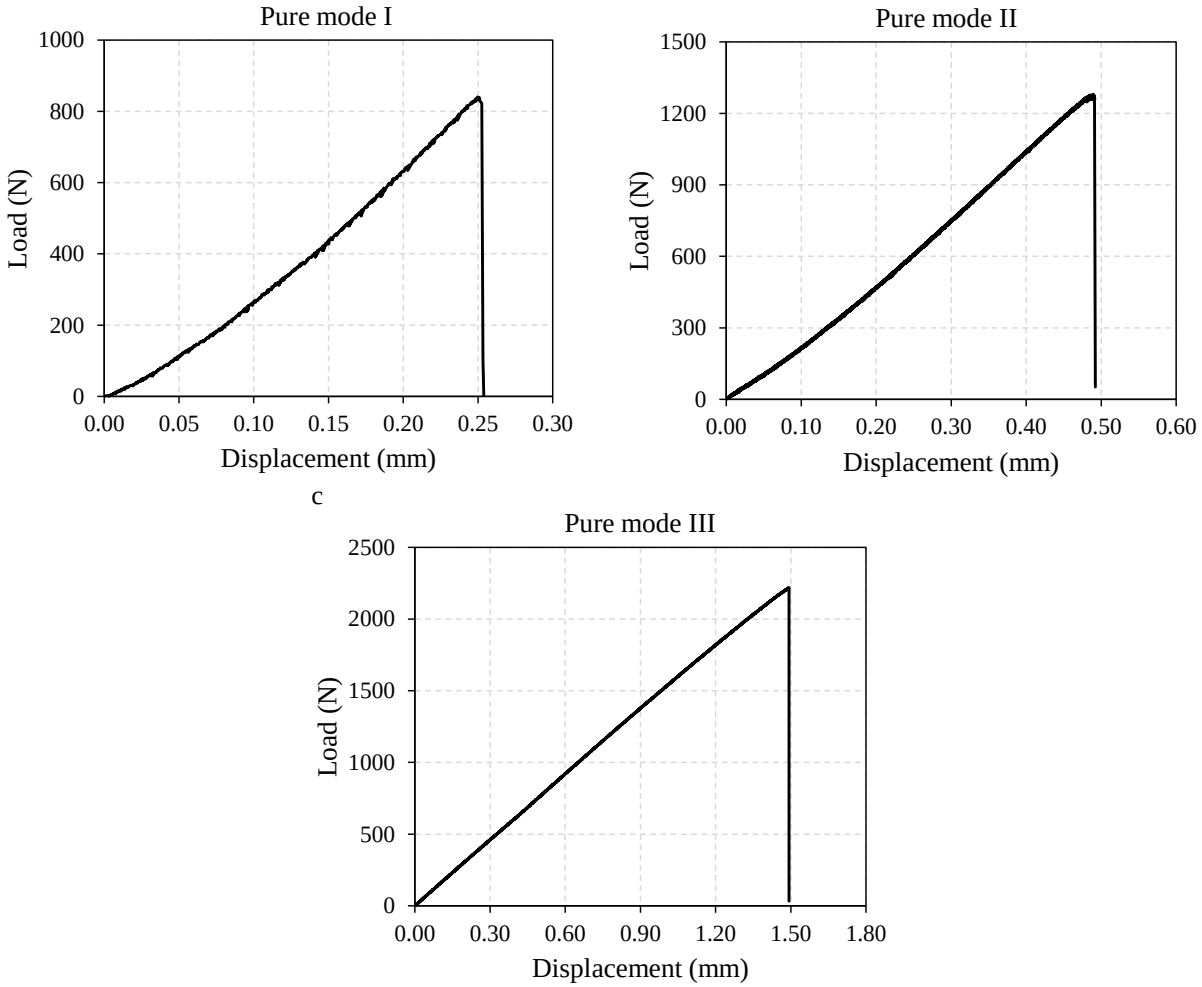

Fig. 13. Representative load–displacement curves obtained from the PMMA samples under different pure fracture mode conditions (a) mode I, (b) mode II, and (c) mode III.

6. Results and discussions

The peak values of the load-displacement curves were extracted and considered as fracture loads of the tested specimens. These values were then used for calculating the critical SIF values from the FE analysis. The details of the fracture tests conducted under different loading conditions are presented in Table 2. In this table, F_c represents the average fracture load while K_{If}, K_{IIf}, K_{IIIf}, and $K_{eff}|_f$ represent critical mode I, mode II, mode III and effective SIFs corresponding to the fracture loads and obtained from the mid-section of the FE models. The critical SIFs under pure fracture modes are called fracture toughness in the current research. The average fracture toughness of PMMA under pure mode I (K_{IC}), pure mode II (K_{IIC}), and pure mode III (K_{IIIC}) were obtained as 18.22 $\text{MPa}\sqrt{\text{mm}}$, 36.77 $\text{MPa}\sqrt{\text{mm}}$, and 102.50 $\text{MPa}\sqrt{\text{mm}}$, respectively.

Table 2. Summary of mixed mode I/II/III fracture tests conducted on PMMA CTS specimens.

Loading mode	α (degree)	β (degree)	F_c (N)	K_{If} ($MPa\sqrt{mm}$)	K_{IIf} ($MPa\sqrt{mm}$)	K_{IIIf} ($MPa\sqrt{mm}$)	$K_{eff}\|_f$ ($MPa\sqrt{mm}$)
I	0	0	796.8 ± 86.8	18.22	0	0	18.22
I/II	22.5	0	833.0 ± 18.5	20.09	5.124	0	20.73
I/II	45	0	779.7 ± 79.3	16.55	10.81	0	19.77
I/II	67.5	0	976.8 ± 75.0	14.52	22.58	0	26.85
II	90	0	1295.4 ± 13.7	0	36.77	0	36.77
I*	0	0	796.8 ± 86.8	18.22	0	0	18.22
I/III	0	22.5	928.2 ± 78.2	22.39	0	2.71	22.55
I/III	0	45	1285.9 ± 76.9	36.73	0	9.70	37.99
I/III	0	67.5	1174.4 ± 30.0	41.65	0	24.44	48.29
III	0	90	2180.1 ± 219.2	0	0	102.50	102.50
II*	90	0	1295.4 ± 13.7	0	36.77	0	36.77
II/III	90	22.5	1189.9 ± 51.2	0	34.79	7.05	35.50
II/III	90	45	1277.9 ± 57.7	0	39.95	18.81	44.16
II/III	90	67.5	1519.2 ± 132.4	0	43.33	47.60	64.37
III*	0	90	2180.1 ± 219.2	0	0	102.50	102.50
I/II/III	22.5	22.5	928.5 ± 36.6	22.24	5.92	2.94	23.20
I/II/III	22.5	45	1090.3 ± 73.4	30.79	7.68	8.91	32.96
I/II/III	22.5	67.5	1075.4 ± 30.0	36.41	9.73	23.89	44.62
I/II/III	45	22.5	877.2 ± 106.3	19.62	12.57	3.48	23.56
I/II/III	45	45	1025.0 ± 35.1	26.67	16.22	10.37	32.89
I/II/III	45	67.5	1070.4 ± 60.4	29.98	19.17	27.41	44.92
I/II/III	67.5	22.5	972.4 ± 62.6	15.19	23.19	5.03	28.17
I/II/III	67.5	45	1116.1 ± 116.5	19.89	28.81	14.49	37.89
I/II/III	67.5	67.5	1255.0 ± 64.5	21.47	31.69	36.84	53.13

* previously presented in the current table.

The critical SIFs resulted from mixed mode I/II/III fracture tests are illustrated in Fig. 14. Also plotted in this figure are the theoretical predictions based on the Richard fracture criterion[30] by considering α_1=0.50 and α_2=0.18. According to Richard criterion, when $K_v=K_{IC}$ brittle fracture occurs. According to Fig. 14, there is relatively good agreement between the experimental data and the theoretical predictions based on Richard criterion. Apart from the mixed mode cases of (α=0°, β=45°) and (α=0°, β=67.5°) with higher discrepancy between the experimental data and the theoretical predictions, theoretical predictions based on Richard criterion followed the experimental data for the rest of the mixed mode loading conditions. Compared to the mode I loading condition, higher fracture toughness values were obtained for the tested PMMA under mode II and mode III loading conditions. One may relate this behavior to the plastic deformation around the crack tip. Hence, in order to have a rough comparison between various loading

conditions, the plastic region around the crack tip was obtained based on von Mises yield criterion[53] considering the yield strength of 60 MPa for PMMA. Fig. 15 shows the shape and the size of plastic zone around the crack tip for some loading conditions. The plastic zones were taken from the surface of FE models (z/t=0) under the average corresponding fracture loads in each loading condition. According to Fig. 15, larger plastic zones were resulted in the specimens with higher in-plane and out of plane loading ratio. The approximate size of the plastic zone for the model under mode I was in the micro order of magnitude, while bigger plastic zones in the order of hundred micro and millimeter were obtained for mode II and mode III, respectively. It is worth mentioning that larger plastic zones dissipate more energy and consequently result in higher fracture toughness values. This is consistent with the previous findings by scholars about mixed mode I/II and mixed mode I/III fracture.[23, 54, 55]

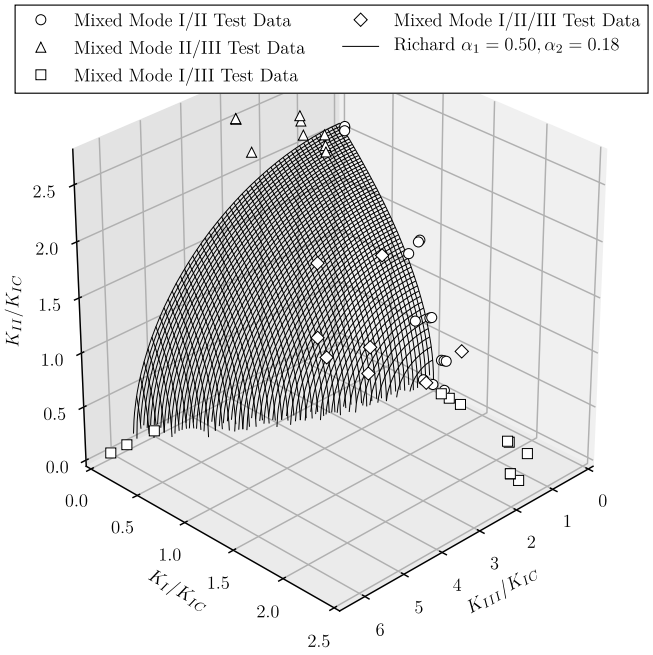

Fig. 14. The critical SIF results obtained from mixed mode I/II/III fracture tests on PMMA using the proposed fixture compared with theoretical predictions by Richard criterion.

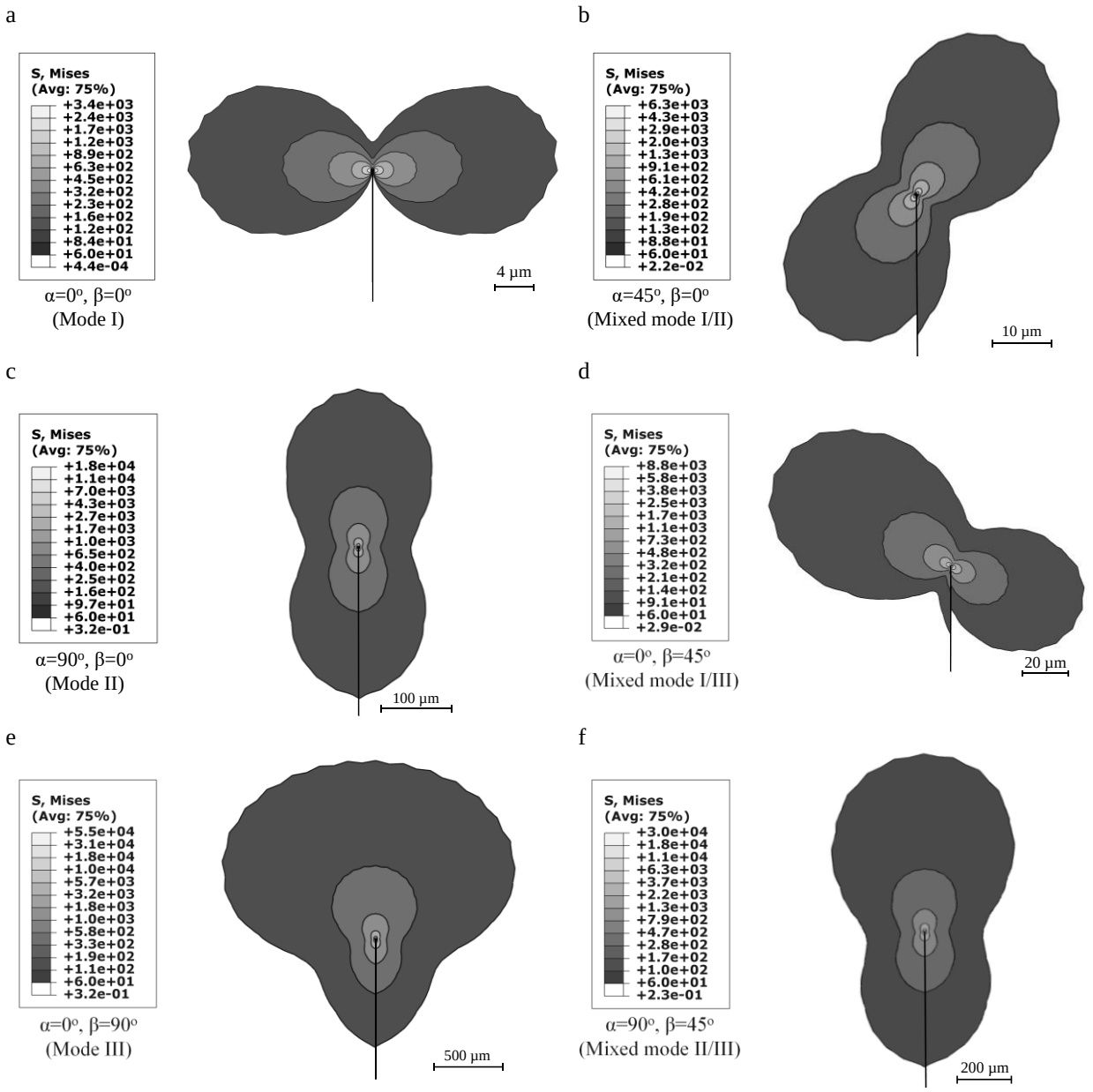

Fig. 15. Plastic zone formed around the crack tip for different loading modes under the average experimental fracture load of each case.

Fig. 16 illustrates the tested specimens under different mixed mode loading conditions. The in-plane and out of plane fracture angles, θ_f, ϕ_f were directly measured at the crack initiation point (i.e. $a/W = 0.5$) by an optical microscope (OptoSigma, osMS26-100, Tokyo-Japan) and the results are presented in Table 3. According to the experimental results, except the pure mode I loading case which crack extension occurred along the initial crack plane, in mixed mode I/II loading condition the crack kinks in the loading plane and in mixed mode I/III loading the crack twists

with respect to the initial crack plane. A combination both in-plane and out of plane crack extension was observed for the case of mixed mode II/III and the general cases of mixed mode I/II/III. For sake of comparison, the theoretical predictions of fracture angles obtain from Eqs. 4 and 5 are also reported in Table 3. Relatively good agreement can be observed between the experimental observations and theoretical predictions.

The discrepancies between the experimental data and theoretical predictions can be attributed to the accuracy of the method used for measurement of crack kinking angle in the specimens loaded under complex mixed mode loading conditions and also presence of coupled modes of fracture. As explained earlier, dealing with thick test specimens under pure mode II and III, non-zero K_{III} and K_{II} values exist on the specimens' surface which results in inherent complexities in all the loading cases including in-plane and out of plane shear loading. The induced local mode III deformation on both sides of crack front prevents the planar crack extension. The twisting angle on both sides of crack front depends on the thickness of specimen. On the other hand, dealing with the specimens under mode III, induced mode II deformation at both sides of crack front enforces the crack not to propagate along the initial out of plane fracture angle, ϕ_f. and results in a nonplanar fracture surface. It is worth mentioning that the coupling mode for the specimens under out of plane loading is considerably higher than in-plane loading. Observation of the curvilinear crack trajectory in the mentioned loading cases is a difficult task which requires further studies. Additional investigations can be conducted to provide modified theoretical models which are able to predict the mixed mode fracture angles with smaller discrepancies.

The proposed general mixed mode fracture test fixture has the capability to induce various modes of fracture in the test specimens. This fixture is one of the few testing fixtures which have been proposed for mixed mode I/II/III fracture test. The main advantage of the current fixture compared to the previous loading fixtures is its simple design which can be readily produced. Additionally, having the simple geometry, the test specimens can be easily machined and prepared for fracture tests. By use of the same specimen geometry for various cases of mixed mode I/II, I/III and II/III fracture tests, comparison of fracture behavior of materials under various loading condition regardless of the geometry effect would be possible. Different loading modes can be obtained using uniaxial loading of the proposed fixture only by choosing different loading holes for the inner part (C-fixture) and outer part (J-fixture). According to the advantages which was pointed

out, the proposed loading fixture can be recommended as a test set-up for performing fracture tests on various engineering materials under any combination of loading modes including, tension-shear (I/II), tension-tear (I/III), shear-tear (II/III), and general tension-shear-tear (I/II/III). The proposed testing fixture can be used for both for metallic and non-metallic materials and the results can be employed for evaluating new fracture prediction criteria under various loading modes.

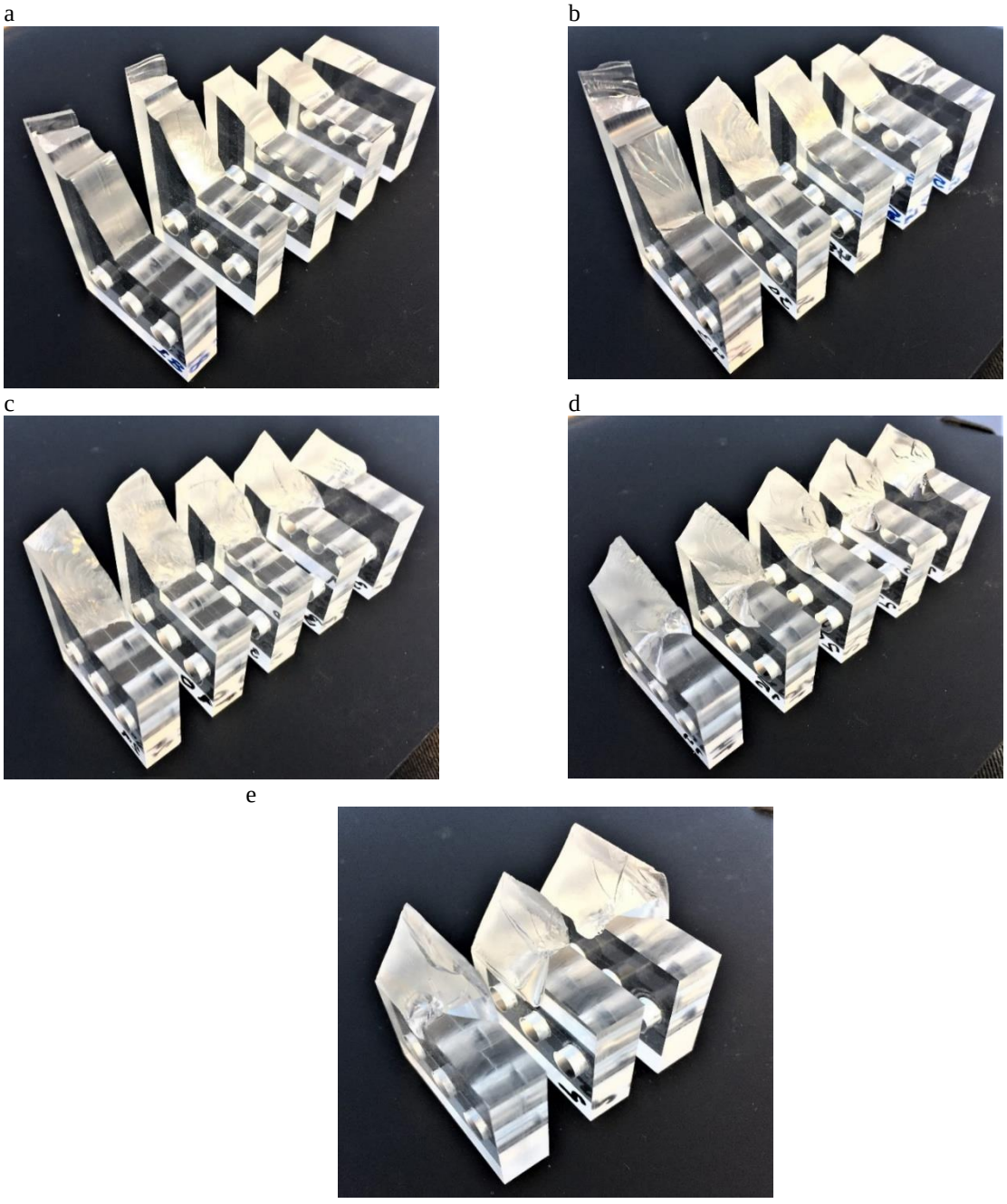

Fig. 16. CTS specimens fractured under different loading conditions, with α=0^{o} on the right and α=90^{o} on the left side of the pictures; (a) β=0^{o}, (b) β=22.5^{o}, (c) β=45^{o}, (d) β=67.5^{o}, (e) β=90^{o}.

Table 3. Summary of experimental and theoretical values of mixed mode I/II/III fracture angles.

Loading mode	α (degree)	β (degree)	$\theta_f\|_{EXP.}$ (degree)	$\phi_f\|_{EXP.}$ (degree)	$\theta_f\|_{THEOR.}$ (degree)	$\phi_f\|_{THEOR.}$ (degree)	θ_f discrepancy	ϕ_f discrepancy
I	0	0	0	0	0	0	0	0
I/II	22.5	0	21.29	0	25.56	0	20	0
I/II	45	0	35.15	0	44.39	0	26	0
I/II	67.5	0	55.71	0	59.28	0	6	0
II	90	0	68.19	0	70.00	0	3	0
I*	0	0	0	0	0	0	0	0
I/III	0	22.5	0	19.23	0	8.04	0	58
I/III	0	45	0	37.08	0	14.86	0	60
I/III	0	67.5	0	46.71	0	24.33	0	48
III	0	90	0	42.02	0	45.00	0	7
II*	90	0	68.19	0	70.00	0	3	0
II/III	90	22.5	53.80	10.41	68.01	12.21	26	17
II/III	90	45	47.92	16.02	62.83	21.59	31	35
II/III	90	67.5	37.53	40.05	50.82	31.79	35	21
III*	0	90	0	42.02	0	45.00	0	7
I/II/III	22.5	22.5	33.83	8.00	24.11	7.08	29	12
I/II/III	22.5	45	18.04	31.84	20.85	13.50	16	58
I/II/III	22.5	67.5	15.42	48.96	18.10	22.77	17	53
I/II/III	45	22.5	45.99	9.36	40.64	7.30	12	22
I/II/III	45	45	25.03	18.47	36.14	13.94	44	25
I/II/III	45	67.5	32.18	44.39	30.67	23.70	5	47
I/II/III	67.5	22.5	67.13	10.17	54.81	8.59	18	16
I/II/III	67.5	45	42.73	13.67	49.28	16.15	15	18
I/II/III	67.5	67.5	44.25	38.25	40.62	26.40	8	31

* previously presented in the current table.

7. Conclusions

A new loading fixture was proposed for general mixed mode I/II/III fracture studies. Three-dimensional finite element analyses were performed on the designed set-up and the results revealed that the loading fixture is capable of providing pure mode I, pure mode II, pure mode III and a favorable distribution of mixed mode I/II, I/III, II/III and I/II/III among them. A series of general mixed mode fracture tests were performed on CTS specimens made of PMMA to practically confirm the performance and efficiency of the proposed fixture. Fracture loads and fracture angles were obtained from the experiments and the results were compared with the theoretical predictions based on Richard criterion. Relatively good agreement was found between the experimental and theoretical results. The proposed fracture test fixture and its associated CTS test specimen is recommended as a practical and suitable test set-up for any type of mixed mode fracture studies.

Declaration of conflicting interests

The authors declared no potential conflicts of interest with respect to the research, authorship, and/or publication of this article.

Funding

The authors received no financial support for the research, authorship, and/or publication of this article.

References

[1] Seed GM, Nowell D. Use of the distributed dislocations method to determine the T-stress. Fatigue Fract Eng Mater Struct. 1994;17(5): 605-618.

[2] Richard HA, Benitz K. A loading device for the creation of mixed mode in fracture mechanics. Int J Fracture. 1983;22: R55-R58.

[3] Arcan M, Hashin Z, Volosnin A. A method to produce uniform plane-stress states with application to fibre-reinforced materials. Exp Mech. 1978;18: 141-146.

[4] Marsavina L, Linul E, Voiconi T, Constantinescu DM, Apostol DA. On the crack path under mixed mode loading on PUR foams. Frattura ed Integrita Strutturale. 2015;9(34): 387-396.

[5] Williams JG, Ewing PD. Fracture under complex stress – the angled crack problem. Int J Fracture. 1972;8: 441-446.

[6] Ueda Y, Ikeda K, Kao T, Aoki M. Characteristics of brittle fracture under general combined modes including those under bi-axial tensile loads. Engng Fract Mech. 1983;18: 1131-1158.

[7] Awaji H, Sato S. Combined mode fracture toughness measurement by the disc test. J Eng Mater Technol. 1978;100: 175-182.

[8] Shetty DK, Rosenfield AR, Duckworth WH. Mixed-mode fracture in biaxial stress state: application of the diametral-compression (Brazilian disk) test. Eng Fract Mech. 1987;26(6): 825-840.

[9] Fett T, Gerteisen G, Hahnenberger S, Martin G, Munz D. Fracture tests for ceramics under mode-I, mode-II and mixed-mode loading. J Eur Ceram Soc. 1995;15: 307-312.

[10] Suresh S, Shih CF, Morrone A, O-Dowd NP. Mixed-mode fracture toughness of ceramic materials. J Am Ceram Soc. 1990;73(5): 1257-1267.

[11] Marsavina L, Constantinescu DM, Linul E, Stuparu FA, Apostol DA. Experimental and numerical crack paths in PUR foams. Eng Fract Mech. 2016;167: 68-83.

[12] Gómez FJ, Elices M, Berto F, Lazzarin P. Local strain energy to assess the static failure of U-notches in plates under mixed mode loading. Int J Fract. 2007;145: 29–45.

[13] Gómez FJ, Elices M, Berto F,·Lazzarin P. Fracture of V-notched specimens under mixed mode (I + II) loading in brittle materials. Int J Fract. 2009;159: 121–135.

[14] Lim IL, Johnston IW, Choi SK, Boland JN. Fracture testing of a soft rock with semi-circular specimens under three-point bending, part 2 – mixed mode. Int J Rock Mech Min Sci Geomech Abstr. 1994;31(3): 199-212.

[15] Berto F, Ayatollahi MR, Borsato T, Ferro P. Local strain energy density to predict size-dependent brittle fracture of cracked specimens under mixed mode loading. Theor Appl Fract Mech. 2016;86: 217–224.

[16] Yukio U, Kazuo I, Tetsuya Y, Mitsuru A. Characteristics of brittle fracture under general combined modes including those under bi-axial tensile loads. Eng Fract Mech. 1983;18: 1131-1158.

[17] Pook L. The fatigue crack direction and threshold behaviour of mild steel under mixed mode I and III loading. Int J Fatigue. 1985;7: 21-30.

[18] Kamat S, Srinivas M, Rama Rao P. Mixed mode I/III fracture toughness of Armco iron. Acta mater. 1998;46: 4985-4992.

[19] Kumar A, Hirth J, Hoagland R, Xiaoxin F. A suggested test procedure to measure mixed mode I-III fracture toughness of brittle materials. J Test Eval. 1994;22: 327-334.

[20] Cooke ML, Pollard DD. Fracture propagation paths under mixed mode loading within rectangular blocks of polymethyl methacrylate. J Geophys Res. 1996;101: 3387-3400.

[21] Chang J, Xu J, Mutoh Y. A general mixed-mode brittle fracture criterion for cracked materials. Eng Fract Mech. 2006;73: 1249-1263.

[22] Lin B, Mear M, Ravi-Chandar K. Criterion for initiation of cracks under mixed-mode I+ III loading. Int J Fract. 2010;165: 175-188.

[23] Ayatollahi MR, Saboori B. A new fixture for fracture tests under mixed mode I/III loading. Eur J Mech A Solids. 2015;51: 67-76.

[24] Hellier AK, McGirr MB, Corderoy DJH. A finite element and fatigue threshold study of shelling in heavy haul rails. Wear. 1991;144: 289–306.

[25] Fajdiga G, Sraml M, Flasker J. *Surface Fatigue of Gear Teeth Flanks*. In: Fracture of Nano and Engineering Materials and Structures. Edited by: Gdoutos EE. Springer, Netherlands; 2006, 197–198.

[26] Hellier AK, Corderoy DJH, McGirr MB. A practical mixed Mode II/III fatigue test rig. Int J Fatigue. 1987;9: 95–101.

[27] Merati AA, Hellier AK, Zarrabi K. On the mixed Mode II/III fatigue threshold behaviour for aluminium alloys 2014–T6 and 7075–T6. Fatigue Fract Eng Mater Struct. 2012;35: 2–12.

[28] Saboori B, Ayatollahi MR. A novel test configuration designed for investigating mixed mode II/III fracture. Eng Fract Mech. 2018;197: 248-258.

[29] Richard HA, Kuna M. Theoretical and experimental study of superimposed fracture modes I, II and III. Eng Fract Mech. 1990;35(6): 949-960.

[30] Richard HA, Schramm B, Schirmeisen NH. Cracks on mixed mode loading – theories, experiments, simulations. Int J Fatigue. 2014;62: 93-103.

[31] Zeinedini A. A novel fixture for mixed mode I/II/III fracture testing of brittle materials. Fatigue Frac Eng mater Struct. (in press). https://doi.org/10.1111/ffe.12955

[32] Pook LP. *The significance of mode I branch cracks for combined mode failure*. In: Radon JC, editor. Fracture and fatigue: elasto-plasticity, thin sheet and micromechanism problems. Oxford: Pergamon Press; 1980, 143–153.

[33] Pook LP. *Comments and fatigue crack growth under mixed modes I and III and pure mode III loading*. In: Miller KJ, Brown MW, editors. Multiaxial fatigue, ASTM STP853. Philadelphia: American Society for Testing and Materials; 1985, 249–263.

[34] Zhao Y. A strain energy criterion for mixed mode crack propagation. Eng Fract Mech. 1987;26: 533-539.

[35] Zhao Y. Griffith's criterion for mixed mode crack propagation. Eng Fract Mech. 1987;26: 683-689.

[36] Sih GC. *Mechanics of fracture initiation and propagation: surface and volume energy density applied as failure criterion*. Springer Science & Business Media, Dordrecht, 1991. https://doi.org/10.1007/978-94-011-3734-8.

[37] Pook LP. *Linear elastic fracture mechanics for engineers: theory and application*. Southampton: WIT Press, 2000.

[38] Schöllmann M, Richard H, Kullmer G, Fulland M. A new criterion for the prediction of crack development in multiaxially loaded structures. Int J Fract. 2002;117: 129-141.

[39] ABAQUS (2018) `ABAQUS/CAE 6.14 User's Manual', Dassault Systèmes, Providence, RI, USA.

[40] Kotousov A, Lazzarin P, Berto F, Pook LP. Three-dimensional stress states at crack tip induced by shear and anti-plane loading. Eng Fract Mech. 2013;108: 65–74.

[41] Pook LP, Campagnolo A, Berto F, Lazzarin P. Coupled fracture mode of a cracked plate under anti-plane loading. Eng Fract Mech. 2015;134: 391-403.

[42] Pook LP, Berto F, Campagnolo A, Lazzarin P. Coupled fracture mode of a cracked disc under anti-plane loading. Eng Fract Mech. 2014;128: 22-36.

[43] Berto F, Lazzarin P, Wang CH. Three-dimensional linear elastic distributions of stress and strain energy density ahead of V-shaped notches in plates of arbitrary thickness. Int J Fract. 2004;127(3): 265-282.

[44] Berto F, Lazzarin P, Kotousov A. On the presence of the out-of-plane singular mode induced by plane loading with K II = K I = 0. Int J Fract. 2011;167(1):119-126.

[45] Kotousov A, Berto F, Lazzarin P, Regorin F. Three dimensional finite element mixed fracture mode under anti-plane loading of a crack. Theor Appl Fract Mech. 2012;62(1):26-33.

[46] Berto F, Lazzarin P, Kotousov A, Harding S. Out-of-plane singular stress fields in V-notched plates and welded lap joints induced by in-plane shear load conditions. Fatigue Fract Eng Mater Struct. 2011;34(4):291-304.

[47] Kotousov A, Lazzarin P, Berto F, Harding S. Effect of the thickness on elastic deformation and quasi-brittle fracture of plate components. Eng Fract Mech. 2010;77(11):1665-1681.

[48] Pook. A 50-year retrospective review of three-dimensional effects at cracks and sharp notches. Fatigue Fract Eng Mater Struct. 2013;36:699-723.

[49] Zhu L, Li Q, Buchholz FG. Computational fracture analysis of an AFM-specimen under mixed mode loading conditions. J Mar Sci Appl. 2011;10: 105–112.

[50] Buchholz FG, Chergui A, Richard H. Fracture analyses and experimental results of crack growth under general mixed mode loading conditions. Eng Fract Mech. 2004;71: 455–468.

[51] Ayatollahi MR, Razavi SMJ, Moghaddam MR, Berto F. Mode I fracture analysis of polymethylmetacrylate using modified energy-based models. Phys Mesomech. 2015;18(4): 326-336.

[52] Ayatollahi MR, Moghaddam MR, Razavi SMJ, Berto F. Geometry effects on fracture trajectory of PMMA samples under pure mode-I loading. Eng Fract Mech. 2016;163: 449-461.

[53] Gdoutos E, Papakaliatakis G. Crack growth initiation in elastic-plastic materials. Int J Fract. 1986;32: 143-156.

[54] Kudari S, Maiti B, Ray K. The effect of specimen geometry on plastic zone size: a study using the J integral. J Strain Anal Eng Des. 2007;42: 125-136.

[55] Sharanaprabhu C, Kudari S. Finite element analysis of minimum plastic zone radius criterion for crack initiation direction under mixed mode loading. In: AIP Conference Proceedings, 2009:3.